Water Hammer Modelling: Advanced Modelling in Science Final Project Report

Kelvin Loh (4248376) - TUD
Kevin Verhaegh (0658453) TU/e
Nick Gaiko (4246721) - TUD
Tugce Akkaya (4246527) - TUD

MasterMath

k.k.l.loh@student.tudelft.nl
April 28, 2013

Abstract

In this report, the full Fluid-Structure Interaction (FSI) problem with a focus in water hammer phenomena is explored. An exact solution to the problem is obtained by using a simple recursion algorithm written in MATLAB. The method of obtaining the solution is accelerated by parallelization. The applicability of such methods have been explored by a fictional optimization case study, which seeks to demonstrate a use of this model in practical engineering pipe design problems.

1 Introduction

Fluid-Structure Interaction (FSI) is a vast field. Depending on the problem, the fluid and structure equations can be fully linearized for small oscillations, as is the case for the water hammer phenomenon with inviscid and isothermal assumptions. On the other end of the spectrum, there are the general problems of transient fluid structure interaction with large changes to the fluid domain due to structural motion,

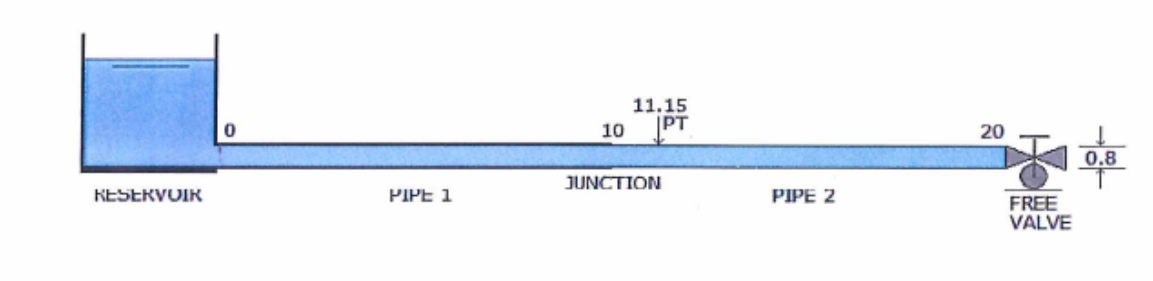

Figure 1: Sketch of reservoir-pipe-valve system

and where the fluid also behaves nonlinearly with viscous and thermal effects taken into account. As this is a short duration project, the simpler assumption of the first case which allows linearization of the resulting coupled partial differential equations is used for this project.

The water hammer effect can be described as follows. When steady flow in a pipe is suddenly stopped by closing a valve, the pressure at the valve will rise and travel upstream as a pressure shock wave. The pressure rise can be substantial. As an example, stopping water flowing at 0.1 m/s can result in a pressure rise of 0.1 MPa inside the pipe. This results in a huge hammering force acting on the valve. If the valve is not rigidly anchored, it will move. Even if the valve can be rigidly fixed, the forces acting on the fixing brackets will be very high. For flexible valves, the motion of the valve will reduce the initial pressure rise, but it can amplify later pressure variations. This is a simple example of fluid-structure interaction (FSI) where the transient fluid flow and the valve vibration affect each other. This phenomenon is especially important in aerospace applications where the vibrations inside the propellant feed system of a spacecraft can induce undesirable motions of the spacecraft in space (nearly undamped), making it difficult to determine the true orientation or trajectory of the spacecraft.

In this project a mathematical model of pressure waves in the fluid and their interaction with valve vibration is developed. The solutions of the model gives insight into the physics of the problem. Figure 1 shows the schematic of the problem investigated by this project.

2 Mathematical Modeling

The dynamics of fluids is often described by the Navier-Stokes equations [1], which are a set of partial differential equations that consist out of the continuity relation and the momentum balance equation. First, the continuity and momentum balance equations are used to create 1D governing equations for the liquid pipe flow. Secondly, the structural governing equations (stress-strain relations) are applied on the pipe, to create 1D governing relations for the pipe. The four resulting equations with four unknowns gives a model that takes fluid-structure interaction into account by coupling the fluid and pipe equations with their respective source terms.

This model can be simplified by assuming that the relations of the pipe are quasi-static, which means that the acceleration of the pipe in radial direction is negligible. This simplification gives rise to equations relating the stress parameters of the pipe and the pressure of the liquid, which simplifies the full model into a four-equation model that takes fluid-structure interaction into account [2].

The effect of the valve is included by using the valve as a boundary condition for the four-equation model. In this case the fluid, structure and valve interaction is taken into account.

2.1 Fluid dynamics

The conservation of mass in fluid mechanics, known as the continuity equation (2.1):

$$\frac{\partial \rho}{\partial t} + \nabla \cdot (\rho \vec{V}) = 0 \tag{2.1}$$

The Navier-Stokes equation, equation (2.2) is a formulation of the momentum equation and an application of Newton's second law using an Eulerian frame.

$$\frac{\partial \rho \vec{V}}{\partial t} + \nabla \cdot \left(\rho \vec{V} \otimes \vec{V} \right) = -\nabla P + \mu \nabla \cdot \left(\nabla \vec{V} + \left(\nabla \vec{V} \right)^T \right) \tag{2.2}$$

Please refer to Appendix A for the full derivation from the conservation, compressible form of the Navier-Stokes equation to the final form used in this project and also commonly used for water hammer applications.

By assuming that the fluid is nearly incompressible which enables the use of the effective fluid bulk modulus, K_{eff}, which describes the change in density due to a change in pressure ($K_{eff} = \rho_f \frac{\partial p}{\partial \rho_f}$), and the fluid velocity is low compared to the speed of sound in the fluid and solid, (Mach number, $Ma \approx 0$), the conservation of

mass can be rewritten in 2D cylindrical coordinates (and assuming axial symmetry $\frac{\partial}{\partial \phi} = 0$) as:

$$\frac{1}{K_{eff}} \frac{\partial p}{\partial t} + \frac{\partial v_x}{\partial x} + \frac{1}{r} \frac{\partial}{\partial r}(r v_r) = 0 \tag{2.3}$$

A linear model of the equations of motion can be obtained from Navier-Stokes by using 2D cylindrical coordinates, assuming axial symmetry, ignoring convective terms $(\vec{v} \cdot \nabla v)$ and by ignoring viscous effects and gravity (because the pressure gradient is much larger). Neglecting the convective term means that the temporal effect on the flow field is much higher than the spatial effect, which is for example the case in 1D flow. The quantity ρ_f is the fluid density.

$$\begin{aligned} \rho_f \frac{\partial v_x}{\partial t} + \frac{\partial p}{\partial x} &= 0 \\ \rho_f \frac{\partial v_r}{\partial t} + \frac{\partial p}{\partial r} &= 0 \end{aligned} \tag{2.4}$$

In order to simplify the model from 2D to 1D, the conservation of mass and equation of motion in axial direction can be averaged cross-sectionally. The quantities V and P are the cross-sectionally averaged axial velocity and pressure respectively. The equation of motion in radial direction is obtained by $\frac{1}{2\pi R^2} \int_0^R 2\pi r^2 (\rho_f \frac{\partial v_r}{\partial t} + \frac{\partial p}{\partial r}) = 0$. This choice has been made in accordance with classical water-hammering theory (that does not take fluid structure interaction into account). The 2D equation has to be multiplied by r^2 in order to maintain radial information (which is an effect of cylindrical coordinates). Furthermore, if the density does not change much as a function of time and the axial velocity does not change much as a function of position, it follows from the 2D continuity relation that $r v_r = \text{constant}$, which has been used for the derivation of the 1D motion in radial direction. The resulting 1D equations are:

$$\begin{aligned} \frac{1}{K} \frac{\partial P}{\partial t} + \frac{\partial V}{\partial x} + \frac{2}{R} v_r|_{x=R} &= 0 \\ \rho_f \frac{\partial V}{\partial t} + \frac{\partial P}{\partial x} &= 0 \\ \frac{1}{2} \rho_f R \frac{\partial v_r}{\partial t}|_{x=R} + p|_{r=R} - P &= 0 \end{aligned} \tag{2.5}$$

Please refer to Appendix A for the full treatment of the derivation and scaling of the fluid equations.

2.2 Pipe dynamics

Although the pipe dynamics is a description of a solid, the Eulerian form of the conservation laws can also be used to derive the pipe dynamics by treating the pipe as a continuum. The same assumptions are made as in the fluid dynamics. However, in this case there is no pressure gradient but only the stress terms. Only the diagonal of the stress tensor is used, so shear forces are neglected. In order to obtain a linear equation of the stresses, bending stiffness, rotational inertia and structural damping are neglected. The result are two equations describing the motion of the pipe due to external forces.

$$\begin{aligned} \rho_t \frac{\partial \dot{u}_x}{\partial t} &= \frac{\partial \sigma_x}{\partial x} \\ \rho_t \frac{\partial \dot{u}_r}{\partial t} &= \frac{1}{r}\frac{\partial (r\sigma_r)}{\partial r} - \frac{\sigma_\phi}{r} \end{aligned} \tag{2.6}$$

The density of the pipe is ρ_t and the pipe's strain rate is $\vec{\dot{u}}$. The diagonal stress terms in the stress tensor is $\vec{\sigma}$.

The 2D equations of motion are converted to 1D equations of motion by cross-averaging. The cross-averaging is over the cross-section of the pipe, so for a pipe with thickness e it is from $R \to R + e$. This leads to the following equations:

$$\begin{aligned} \rho_t \frac{\partial \overline{\dot{u}_x}}{\partial t} &= \frac{\partial \overline{\sigma}_x}{\partial x} \\ \rho_t \frac{\partial \overline{\dot{u}_r}}{\partial t} &= \frac{R+e}{(R+\frac{1}{2}e)e}\sigma_r|_{r=R+e} - \frac{R}{(R+\frac{1}{2}e)e}\sigma_r|_{r=R} - \frac{1}{R+\frac{1}{2}e}\overline{\overline{\sigma_\phi}} \end{aligned} \tag{2.7}$$

In which $\overline{a(r)}$ means the cross-sectional average of a, and $\overline{\overline{a(r)}}$ means the line-average (over the pipe thickness) of a.

Because the pipe is a continuum, the stresses are all related with each other (e.q. if there a stress in one direction, this influences the stress in other directions as well).

These relations are given by the stress-strain relations, which relates internal forces on the pipe (stress ($\vec{\sigma}$) with pipe deformation (strain $\vec{\epsilon}$). These relations depend on the engineering parameters Young's modulus E and Poisson's ratio ν. If a piece of gum is pulled at both ends, the stretching of the gum is described by Young's modulus. If a piece of gum is compressed from the sides, it will also stretch from both ends, which is described by Poisson's ratio. The stress-strain relations (3D) are:

$$\begin{aligned}\epsilon_x &= \frac{1}{RE}(\sigma_x - \nu(\sigma_\phi + \sigma_r)) \\ \epsilon_\phi &= \frac{1}{RE}(\sigma_\phi - \nu(\sigma_x + \sigma_r)) \\ \epsilon_r &= \frac{1}{RE}(\sigma_r - \nu(\sigma_x + \sigma_\phi))\end{aligned} \tag{2.8}$$

Since strain describes the deformation, it is linked with the gradient of the strain rate inside the pipe, since the internal pipe strain rate leads to deformation. This is described in 2D by:

$$\begin{aligned}\epsilon_x &= \frac{\partial u_x}{\partial x} \\ \epsilon_\phi &= \frac{u_r}{r} \\ \epsilon_r &= \frac{\partial u_r}{\partial r}\end{aligned} \tag{2.9}$$

When this set of equations is combined with the stress-strain relations, this leads to a 2D equation describing the relation between the axial-stress and the displacement of the pipe. Since a 1D model is required, this is transformed into 1D by averaging over the cross-section of the pipe, which leads to:

$$\frac{\partial \overline{\sigma}_x}{\partial t} = E\frac{\partial \overline{\dot{u}_x}}{\partial x} + \nu(\frac{\partial \overline{\sigma_\phi}}{\partial t} + \frac{\partial \overline{\sigma_r}}{\partial t}) \tag{2.10}$$

2.3 Fluid-structure interaction

At this point the equations for the liquid and for the pipe were derived. The fluid-structure interaction comes from the coupling of the two sets of equations via the source terms and also boundary conditions.

At the position where the liquid and the pipe touch ($r = R$) the velocity of the liquid and strain rate of the pipe influence each other and the pressure of the liquid acts as a stress on the pipe. The no-slip condition is used, which implies that on an interface the wall velocity and the fluid velocity is the same due to advection. It has been assumed that outside of the pipe there is a vacuum. The coupling relations are therefore:

$$\begin{aligned} \sigma_r|_{r=R} &= -p|_{r=R} \\ \sigma_r|_{r=R+e} &= 0 \\ \dot{u}_r|_{r=R} &= v_r|_{r=R} \\ \dot{u}_r|_{r=R+e} &= 0 \end{aligned} \tag{2.11}$$

The $\vec{\sigma}$ is oriented normal from the surface, hence the minus sign in front of the pressure (which works in the other direction).

Combining the boundary conditions with the fluid and pipe relations gives a complete model. However, this model is rather big and can be simplified further.

2.4 Four-equation model

When the wavelength of the oscillations in the pipe is long compared to the radius of the pipe, radial pipe velocity only varies slowly and the radial acceleration is negligible. The hoop stress σ_ϕ depends on the time due to the radial acceleration and due to the pressure. In the quasi-static stress approximation only the time dependence of the pressure is taken into account.

The stress relations can now be easily derived by calculating the stress distribution in a pressurized ring by using Lame's equations [2].

In the quasi-static approximation the time depended pressure is inserted into the static pressure of the stress distribution of a pressurized ring. Including this equation in the full model makes it possible to simplify the full model into a four equation model.

$$\begin{aligned} \frac{\partial V}{\partial t} + \frac{1}{\rho_f}\frac{\partial P}{\partial x} &= 0 \\ \frac{\partial V}{\partial x} + [\frac{1}{K} + \frac{2}{E}(\frac{R}{e} + \frac{1+\frac{e}{R}}{2+\frac{e}{R}} + \nu)]\frac{\partial P}{\partial t} &= \frac{2\nu}{E}\frac{\partial \overline{\sigma}_x}{\partial t} \\ \frac{\partial \overline{\dot{u}_x}}{\partial t} - \frac{1}{\rho_s}\frac{\partial \overline{\sigma_x}}{\partial x} &= 0 \\ \frac{\partial \overline{\dot{u}_x}}{\partial x} - \frac{1}{E}\frac{\partial \overline{\sigma}_x}{\partial t} &= -\frac{\nu R}{Ee}\frac{1}{1+\frac{1}{2}\frac{e}{R}}\frac{\partial P}{\partial t} \end{aligned} \tag{2.12}$$

The first two equations of the four equation model describe the dynamics of the axial velocity of the liquid and the pressure, which are related with the axial stress in the pipe. The last two equations of the four equation model describe the dynamics

of the axial pipe strain rate, which are related with the fluid pressure. These cross-relations are an effect of the coupling equations. The smaller size compared to the full model is an effect of the quasi-static approximation. Since equation (2.12) is for the thick-wall FSI model, for a thin-wall assumption, the equations are further simplified, and the following model of Skalak [3] holds. For the project, the model used is by equation (2.13) since we assume that the pipe has a thin wall (i.e. $e << R$).

$$\begin{aligned} \frac{\partial V}{\partial t} + \frac{1}{\rho_f}\frac{\partial P}{\partial x} &= 0 \\ \frac{\partial V}{\partial x} + \left(\frac{1}{K} + \frac{2R}{Ee}\right)\frac{\partial P}{\partial t} - \frac{2\nu}{E}\frac{\partial \overline{\sigma}_x}{\partial t} &= 0 \\ \frac{\partial \overline{\ddot{u}_x}}{\partial t} - \frac{1}{\rho_s}\frac{\partial \overline{\sigma_x}}{\partial x} &= 0 \\ \frac{\partial \overline{\dot{u}_x}}{\partial x} - \frac{1}{E}\frac{\partial \overline{\sigma}_x}{\partial t} + \frac{\nu R}{Ee}\frac{\partial P}{\partial t} &= 0 \end{aligned} \tag{2.13}$$

2.5 Valve boundary conditions

The dynamics of the pipe and liquid are now modelled and the fluid structure interaction is taken into account. However, one major aspect in water hammering is the valve, which has not been taken into account yet. The valve can be taken into account by including it as a boundary condition.

From Bernoulli's equations it can be derived that the pressure difference between a pipe with flowing liquid and the vacuum surroundings (at position $x = L$) is $\Delta P_0|_{x=L} = \frac{1}{2}\rho_f V|V|$. However, this is an approximation, because Bernoulli states that the mechanical energy in a fluid along a streamline is constant. However, this depends on the opening. Sometimes an opening is of such a shape that the streamlines get "lost" and generate turbulent effects. In order to cope with these effects, an empirical factor ξ_0 is introduced in Bernoulli's equation: $\Delta P_0|_{x=L} = \frac{1}{2}\xi_0\rho_f V|V|$.

In tap that is closed as a function of time can be treated in a similar way if the empirical loss factor is taken as a function of time $\xi(t)$. The effect of the movement of the pipe also has to be taken into account and hence the relative speed of the fluid with respect to the pipe strain rate (here it is assumed that the valve moves at the same speed as the pipe) is taken $V \to V - \dot{u}_x$. The effect of the valve is described by a specific function $\tau = \sqrt{\frac{\xi_0}{\xi(t)}}$, which is supplied by the manufacturer.

Since the tap is at the end of the pipe, a fluid particle is stopped at the end of the pipe (and reflected), but at the very end of the pipe, the fluid velocity is zero, which

means that the axial strain at the very end of the pipe is zero as well.

This completes the set of boundary conditions:

$$\begin{aligned} \Delta P|_{x=L} =& \xi_0^2 \tau^2 (V - \dot{u}_x)|V - \dot{u}_x| \\ \sigma_x|_{x=L} =& 0 \end{aligned} \tag{2.14}$$

2.6 Nonlinear non-instantaneous valve

For steady, turbulent pipe flows, the initial pressure loss, ΔP_0 across a fully open valve can be represented by Equation (2.15)

$$\Delta P_0 = \frac{1}{2} \xi_0 \rho_f (V_0 - \dot{U}_{x0})|V_0 - \dot{U}_{x0}| \tag{2.15}$$

$$\Delta P = \frac{1}{2} \xi \rho_f (V - \dot{U}_x)|V - \dot{U}_x| \tag{2.16}$$

The empirical loss coefficient, ξ_0 is described by [5]. Similarly for the closing valve at time, $t > 0$, the relation is given by Equation (2.16). Dividing Equation (2.16) with (2.15) results in the dimensionless valve closure coefficient, $\tau = \sqrt{\frac{\xi_0}{\xi}}$, and the nonlinear relation for the boundary condition

$$P_0 (V - \dot{U}_x)|V - \dot{U}_x| = \tau^2(t)(V_0 - \dot{U}_{x0})|V_0 - \dot{U}_{x0}|P \tag{2.17}$$

with reference pressure downstream of the valve being set to 0.

The valve closure function, $\tau(t)$ is defined from an empirically obtained ball-valve discharge coefficients, provided by Dr. David Wiggert to Delft Hydraulics in 1987 (2.18). More information can be obtained from [6], [7], and [8].

$$\tau(t) = \begin{cases} (1 - t/T_c)^{3.53} & \text{for } 0 \leq t \leq 0.4T_c \\ 0.394(1 - t/T_c)^{1.70} & \text{for } 0.4T_c < t \leq T_c \\ 0 & \text{for } t > T_c \end{cases} \tag{2.18}$$

3 Implementation

There are multiple ways to solve the system of equations (2.13). There is the conventional mesh-based approach via the method of characteristics, finite volume or element methods, and also the more exotic exact, meshless approach.

3.1 Method of Characteristics

The method of characteristics is the conventional method to solve the FSI four-equation model. This is due to the hyperbolic nature of the PDE system, and the wave speeds are constant, while steep wave fronts can be easily resolved as compared to the finite volume or finite element methods. The disadvantage of this method is that the method of characteristics introduces phase error if wave speeds are modified, and numerical dispersion and damping if interpolations are used. Since this method uses a mesh, interpolations becomes necessary when data is required between the mesh points [2].

3.2 Exact (recursive)

The equations (2.13) are solved exactly based on the approach as outlined by Tijsseling [2]. The method tracks the wavefronts backwards in time using a recursion. The method does not require a computational mesh, and thus, data from any point inside the domain can be obtained without interpolation. The disadvantage of this method is that growth in the number of separate waves in the pipe grows exponentially with time. This also means that since each wave needs to be tracked, the algorithm tend to slowdown as it marches in time. However, for this project, the exact solution method is employed for all the cases. Several MATLAB scripts have been written to implement the following algorithm.

3.3 Solution Methodology

The system of equations can be written in the form as shown as (3.1) with $\vec{\Phi}$ as the state space vector representing the primitive variables in the governing equation (2.13). Equation (3.1) can be transformed via eigenvalue decomposition since matrices $\mathbf{A}$ and $\mathbf{B}$ are invertible and $\mathbf{A}^{-1}\mathbf{B}$ is diagonalizable [4]. For the cases in this project, the matrix $\mathbf{C}$ which represents the friction terms are assumed to be $\mathbf{0}$ since a non-zero matrix will cause frequency dispersions and makes the exact solution computation

more difficult to treat.

$$\mathbf{A}\frac{\partial}{\partial t}\vec{\Phi}(x,t) + \mathbf{B}\frac{\partial}{\partial x}\vec{\Phi}(x,t) + \mathbf{C}\vec{\Phi}(x,t) = 0 \tag{3.1}$$

$$\vec{\Phi}(x,t) = \begin{bmatrix} V \\ P \\ \dot{U}_x \\ \sigma_x \end{bmatrix} \tag{3.2}$$

After diagonalization, the system of equations result in equation (3.3)

$$\frac{\partial}{\partial t}\vec{w}(x,t) + \mathbf{\Lambda}\frac{\partial}{\partial x}\vec{w}(x,t) = 0 \tag{3.3}$$

$$\mathbf{\Lambda} = \mathbf{R}^{-1}\mathbf{A}^{-1}\mathbf{B}\mathbf{R} \tag{3.4}$$

$$\vec{w}(x,t) = \mathbf{R}^{-1}\vec{\Phi}(x,t) \tag{3.5}$$

The equations are now decoupled since the matrix $\mathbf{\Lambda}$ is a diagonal matrix representing the wave speeds of the individual waves in the system as shown in equation (3.6). As a result of the decomposition, the matrix $\mathbf{R}$ represent the eigenvectors $\vec{\eta}_i$ of the matrix $\mathbf{A}^{-1}\mathbf{B}$ with the columns corresponding to the entries of the eigenvalue in the matrix $\mathbf{\Lambda}$.

$$\mathbf{\Lambda} = \begin{bmatrix} \lambda_1 & 0 & 0 & 0 \\ 0 & \lambda_2 & 0 & 0 \\ 0 & 0 & \lambda_3 & 0 \\ 0 & 0 & 0 & \lambda_4 \end{bmatrix} \tag{3.6}$$

$$\mathbf{R} = \begin{bmatrix} \vec{\eta}_1 & \vec{\eta}_2 & \vec{\eta}_3 & \vec{\eta}_4 \end{bmatrix} \tag{3.7}$$

The decoupled system of equation (3.6) transforms to equation (3.8)

$$\frac{\mathrm{d}\vec{w}(x,t)}{\mathrm{d}t} = 0 \tag{3.8}$$

along the characteristic lines in the $x - t$ plane as defined by

$$\frac{\mathrm{d}x}{\mathrm{d}t} = \lambda_i\,, \quad i = 1,\ 2,\ 3,\ 4$$

The solution of the ordinary differential equations is then given by equation (3.9) and illustrated by Figure 2

$$w_i(x,t) = w_i(x - \lambda_i\Delta t, t - \Delta t)\,, \quad i = 1,\ 2,\ 3,\ 4 \tag{3.9}$$

Equation (3.9) can be seen with the aid of Figure 2 to be

$$\vec{w}(P) = \begin{pmatrix} w_1(A_1) \\ w_2(A_2) \\ w_2(A_2) \\ w_2(A_2) \end{pmatrix} \tag{3.10}$$

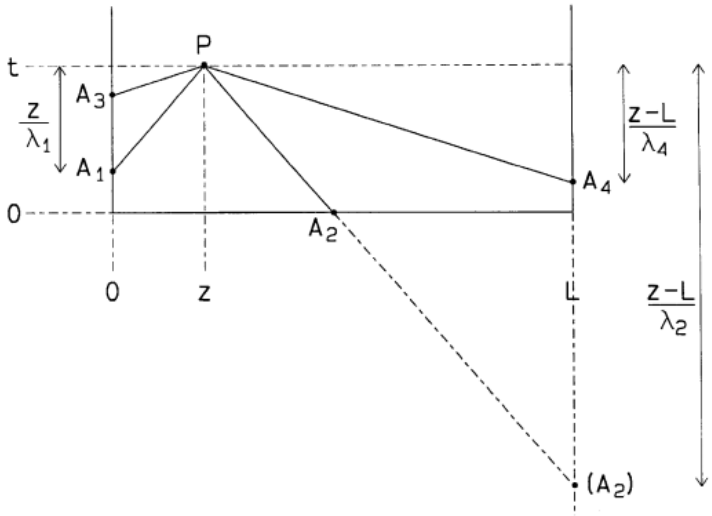

Figure 2: Interior point P and characteristic lines in the $x-t$ plane (Graphic taken from [2])

The primitive variables can then be transformed back to result in Equation (3.11)

$$\vec{\Phi}(P) = \sum_{i=1}^{4} \mathbf{R}\mathbf{S}_i\mathbf{R}^{-1}\vec{\Phi}(A_i) \tag{3.11}$$

where the diagonal i-th element of matrix $\mathbf{S}$ is 1, and all other elements are 0.

The boundary conditions that closes the number of equations and unknowns for this particular project are shown in Equation (3.12). Figure 3 visualizes the idea.

$$\mathbf{D}_b(t)\vec{\Phi}(x_b,t) = \vec{f_b}(t) \tag{3.12}$$

with $\mathbf{D}_b(t) = \begin{bmatrix} 0 & 1 & 0 & 0 \\ 1 & 0 & -1 & 0 \\ 0 & 0 & 1 & 0 \\ 0 & A_f & -c_d & -A_s \end{bmatrix}$, $\vec{f_b} = \begin{pmatrix} 0 \\ 0 \\ 0 \\ 0 \end{pmatrix}$, and $c_d = 0$, the damping coefficient introduced by a dashpot connected to the nonlinear valve.

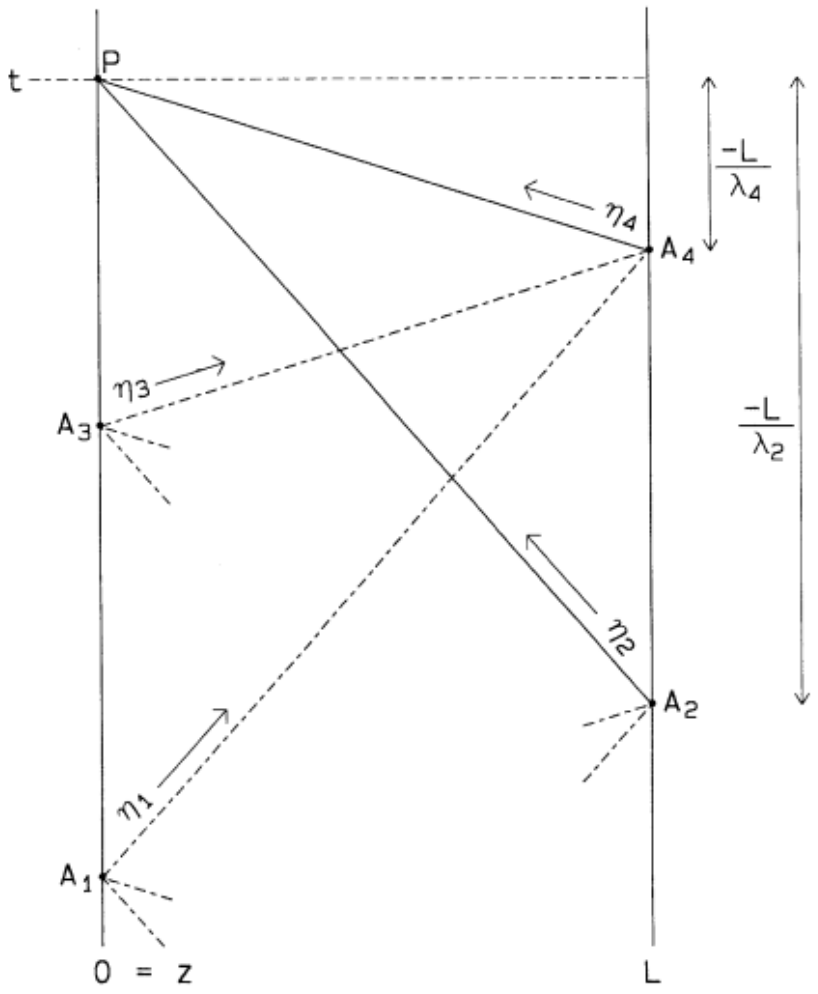

Figure 3: Boundary point P and characteristic lines in the $x-t$ plane (Graphic taken from [2])

3.4 Algorithm

The algorithm to obtain the exact solution for $\vec{\Phi}(x,t)$ at any point (x,t) in the $x-t$ plane is described in [2]. A brief description is described in this report. The algorithm is formulated with regards to the Riemann invariants, $\vec{w}$ along the characteristics. Figure 3 can help in the visualization of the method. For point P on the boundary $x = 0$ at a time t, the Riemann invariant state vector $\vec{w}$ consists of the four components, $w_i, \;\; i = 1,\ 2,\ 3,\ 4$. The known components are assumed to be w_2, and w_4 due to the nature of the characteristics and are equal to the values at A_2, and A_4 respectively, on the boundary at $x = L$. The unknowns w_1, and w_3 are solved from the boundary condition equations (3.12). The same treatment is performed when a point on the boundary $x = L$ at time t is to be solved for. For the calculation of $\vec{w}$ at point P, the past information from points A_2, and A_4 must be known, and for calculating $\vec{w}$ at A_2, and A_4, one also needs an "earlier" information at A_1, and A_3. The entire process is captured by a simple recursion algorithm which stops when the characteristic lines intersect the $t = 0$ line which contains the initial values of the Riemann invariant vector, $\vec{w}$. The full pseudo-code is presented in Appendix B of [2].

3.5 Parallelization

Since the computational time to obtain the solution increases exponentially with the marching of time, the method can be slow. Fortunately, this exact method of solution lends itself very well for parallelization due to the data independence of the points in the $x-t$ plane. It is a very good example of an "embarrassingly parallel" application [9]. As a demonstration of the ease of parallelization of the code, the same MATLAB scripts are modified to use the Parallel Toolbox [10]. The speedup, is defined by Equation (3.13)

$$Speedup = \frac{T_{serial}}{T_{parallel}} \tag{3.13}$$

where T_{serial} is the time to obtain the solution for a single processor, and $T_{parallel}$ is the time to obtain the same solution for a parallel system.

For this case, the speedup is shown in Figure 4. As can be seen, the code does indeed run faster for more number of processors but the speedup is not close to the ideal despite the "embarrassingly parallel" application. This can be explained by the architecture of the computer system in use as the speedup test was run in a laptop with an Intel Core i7 2630QM processor. This processor has a feature which allows it

to increase the core clock speed when running with a single core, effectively increasing the single core performance [11].

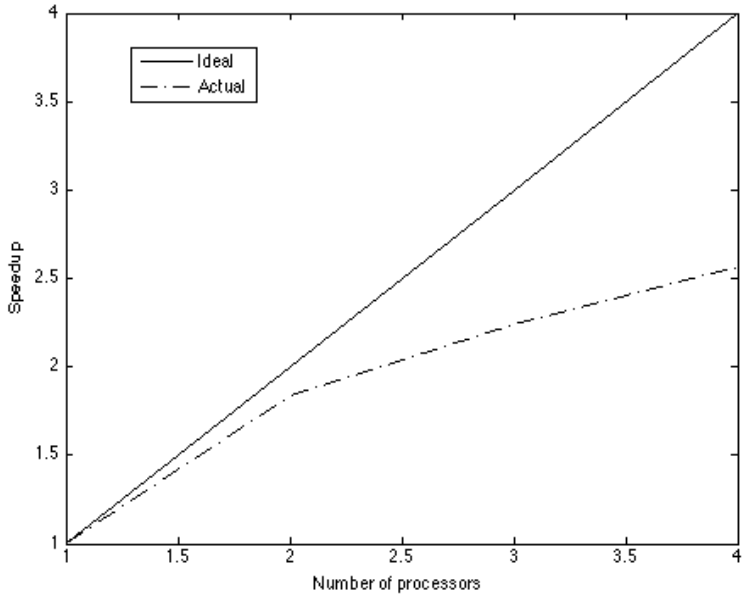

Figure 4: Speedup of the solution using the MATLAB Parallel Toolbox

4 Results and Discussion

For a test case, the Delft Hydraulics Benchmark Problems are defined, and a nonlinear non-instantaneous valve is prescribed at the *free* valve end. The *free* vibrating valve end creates a strong coupling mechanism for fluid-structure interaction. The nonlinear model represented by equation (2.17) is modified to have a forcing vector, $\vec{f_b}(t) = \begin{pmatrix} 0 \\ V_r(t) \\ 0 \\ 0 \end{pmatrix}$ in Equation (3.12). The function $V_r(t) = V - \dot{U}_x$, is obtained by solving the nonlinear boundary condition (2.17) simultaneously, and represents the relative velocity between the absolute fluid velocity and the strain rate of the pipe. Figure 5 shows the valve closure function, $\tau(t)$ for the given problem. Figures 6 and 7 show the fluid velocity profile at the boundary. The results in solid lines are from the realistic

full four equation FSI, while the standard one-way coupling of just solving only for the fluid domain variables are shown in dashed lines. The figures clearly show the effects of the structural interaction with the fluid by having more fluctuations and also, higher absolute maximums as compared to the case of only one-way coupling. Figure 8 shows the internal fluid pressure at the boundaries with comparison between the simplified one-way coupling model and the full FSI two-way coupling model shown. Again, it is shown that the pressure peaks for the two-way coupling model are higher. This can be explained by the beats physical phenomenon since the frequencies of the pressure wave in the fluid and pipe are different. This causes reinforcement of the pressure when the fluid and pipe move anti-phase with one another. A Discrete Fourier Transform is applied to obtain figures 13 to 16. They show the power spectrum of the primitive variables in the system at the valve end. It can be seen that the first primary frequency is at 11.72 Hz, and a second lower amplitude wave at 31.25 Hz. Figures 9 to 12 represent the pipe strain rate, and the pipe internal axial stress respectively at the boundaries. As for the internal point, the test point is at $x = 11.15$ m. Hence, figures 17 to 20 show the profiles of the primitive variables at the required test point.

Table 1: Material properties for the Delft Hydraulics Benchmark Problems

Length, L (m)	20
Inner Radius, R (mm)	398.5
Pipe Thickness, e (mm)	8
Pipe Elastic Modulus, E (GPa)	210
Pipe Density, ρ_s (kg m^{-3})	7985
Pipe Poisson Ratio, ν	0.29
Fluid Bulk Modulus, K_w (GPa)	2.14
Fluid Density, ρ_f (kg m^{-3})	998

4.1 Optimization Case

As a demonstration of one of the uses in the application for this method, an optimization case study is performed. This demonstration serves as an example of the importance of having more accurate physics to help engineers create a lighter, or more cost-effective design. The case study is investigated using the MATLAB Optimization Toolbox [10]. Suppose the fictional requirements of a pipe design are given

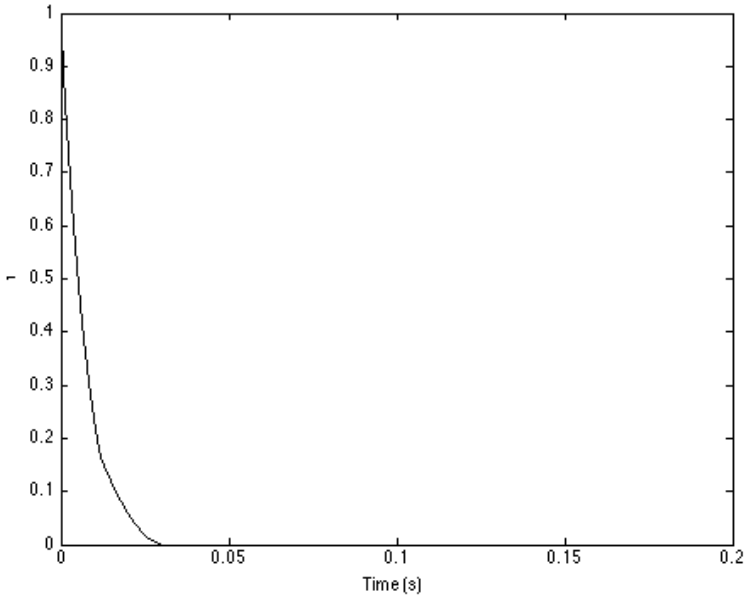

Figure 5: $\tau(t)$ for the problem (Free nonlinear non-instantaneous valve)

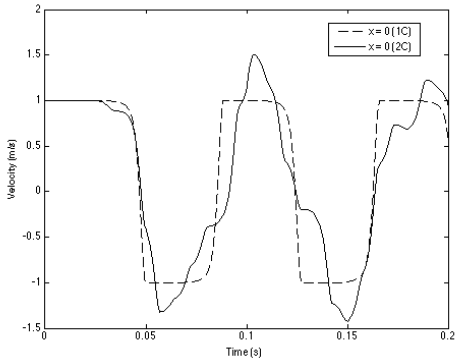

Figure 6: Internal fluid velocity at x = 0 (Free nonlinear non-instantaneous valve)

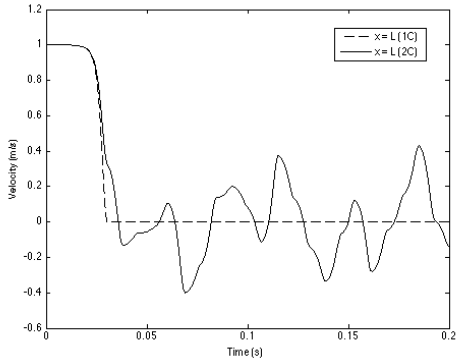

Figure 7: Internal fluid velocity at x = L (Free nonlinear non-instantaneous valve)

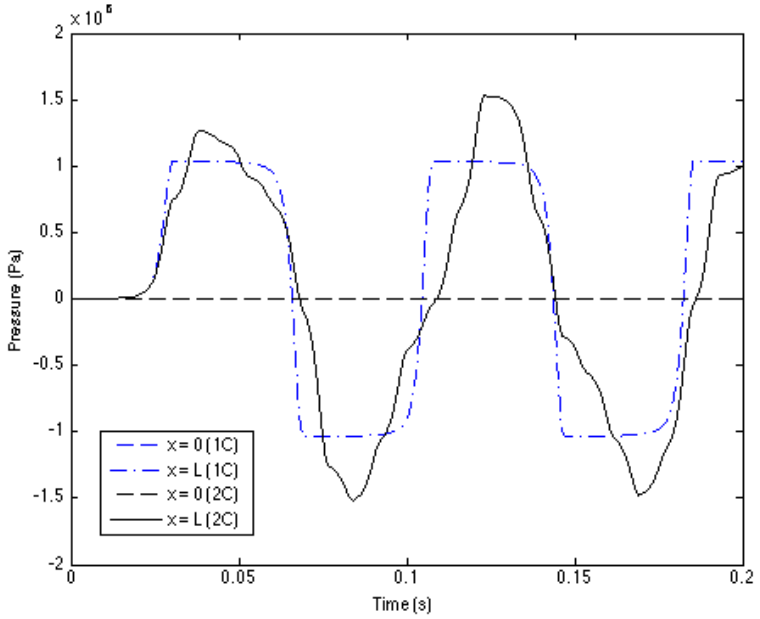

Figure 8: Fluid pressure at the boundaries (Free nonlinear non-instantaneous valve)

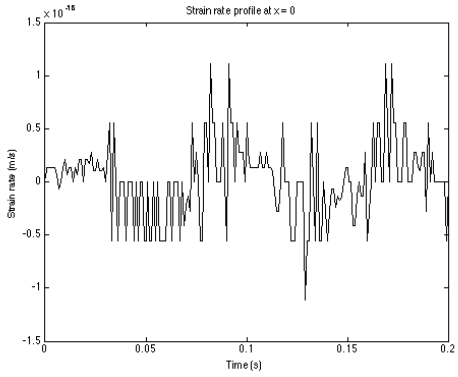

Figure 9: Pipe strain rate at x = 0 (Free nonlinear non-instantaneous valve)

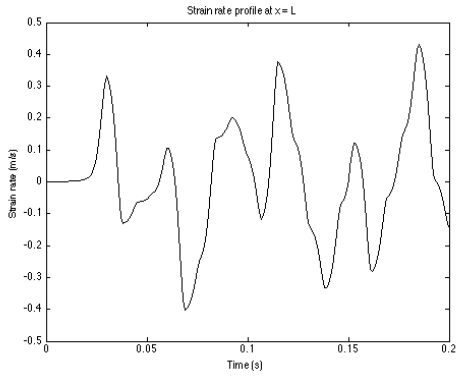

Figure 10: Pipe strain rate at x = L (Free nonlinear non-instantaneous valve)

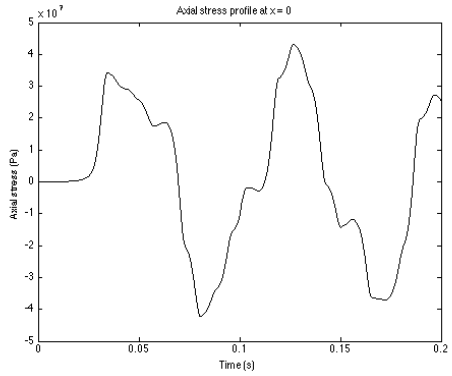

Figure 11: Pipe axial stress at x = 0 (Free nonlinear non-instantaneous valve)

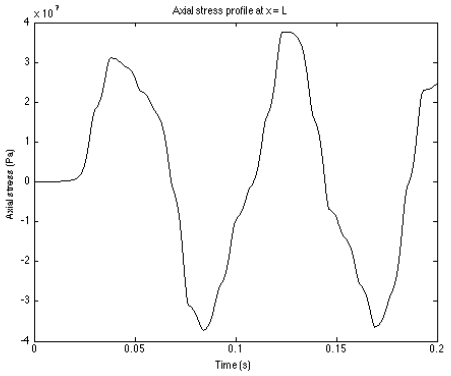

Figure 12: Pipe axial stress at x = L (Free nonlinear non-instantaneous valve)

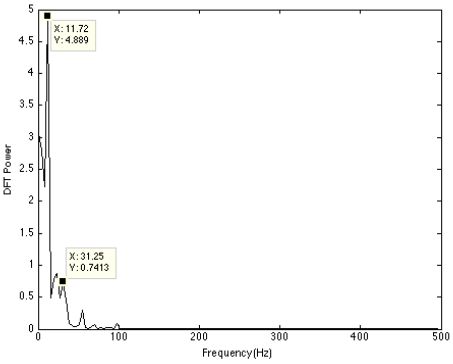

Figure 13: Periodogram of fluid velocity at x = L (Free nonlinear non-instantaneous valve)

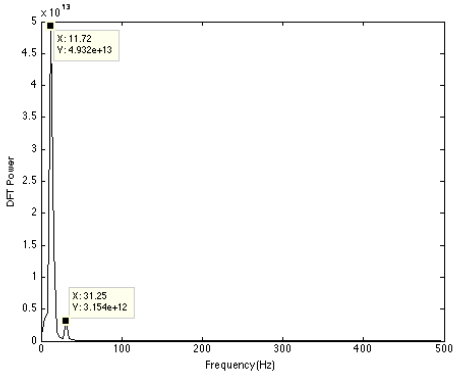

Figure 14: Periodogram of fluid pressure at x = L (Free nonlinear non-instantaneous valve)

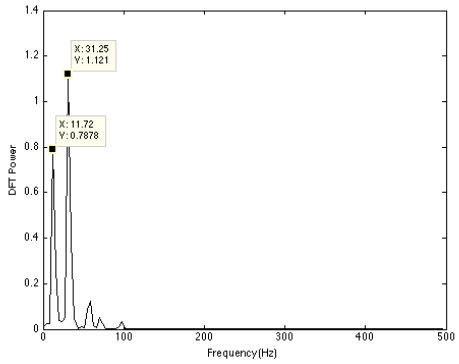

Figure 15: Periodogram of pipe strain rate at x = L (Free nonlinear non-instantaneous valve)

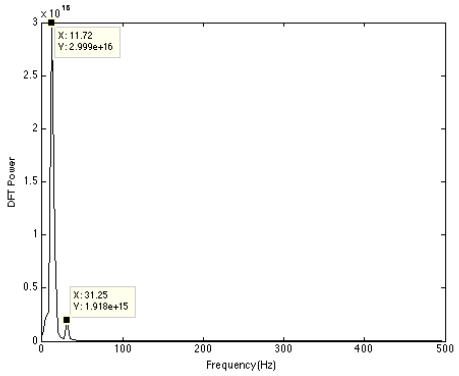

Figure 16: Periodogram of pipe axial stress at x = L (Free nonlinear non-instantaneous valve)

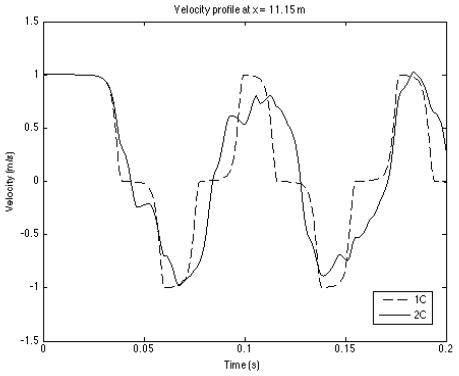

Figure 17: Internal fluid velocity at x = 11.15 m (Free nonlinear non-instantaneous valve)

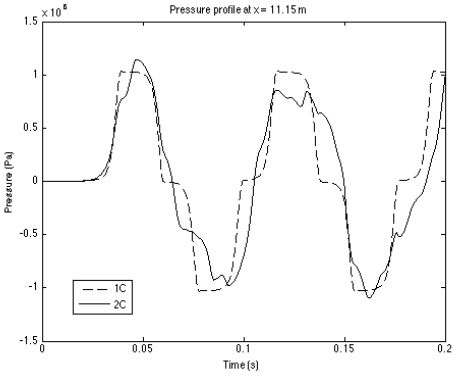

Figure 18: Fluid pressure at x = 11.15 m (Free nonlinear non-instantaneous valve)

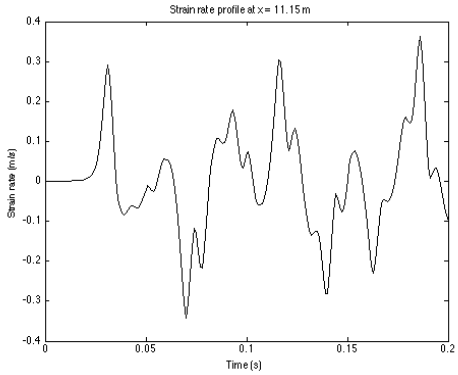

Figure 19: Pipe strain rate at x = 11.15 m (Free nonlinear non-instantaneous valve)

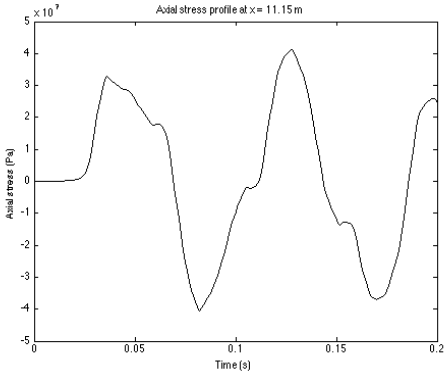

Figure 20: Pipe axial stress at x = 11.15 m (Free nonlinear non-instantaneous valve)

by an engineer in Table 2. The parameters to be optimized for the design are the inner radius, pipe thickness, and valve closure time. This case is then nothing more than a constrained linear optimization problem with nonlinear constraints as defined by the physical model of the coupling between fluid and structural equations. For this particular case study, the objective is to minimize the mass of the pipe while staying within the constraints of the requirements in Table 2. The objective function is defined as equation (4.1) which in this case is nothing more than the mass of the pipe. To achieve this, the MATLAB function *fmincon* is used using an interior point method optimization algorithm with central differencing which also obeys the bounds.

$$J(R, e) = \rho_s \pi \left((R + e)^2 - R^2 \right) \tag{4.1}$$

Since for optimization studies, the simulation must be run multiple times, the simulated time is set at $t = 0.1$ s for each simulation run in order to shorten the computation time to achieve the final design parameters. The simulations are all fully parallelized. The baseline design for comparison and initial conditions for the search algorithm are the existing parameters as outlined by Table 1. Figure 21 shows the output plots for the optimization search algorithm. Figures 22 to 25 shows a comparison between the final design and the baseline design. The initial result from figure 21 shows the baseline design having a mass of 3200 kg. The final design point gives a mass of 724 kg which fulfills all the design constraints. Table 3 gives the parameters found for the final design by the optimization algorithm and the resulting mass. Figure 25 shows an interesting feature in that the peak axial stress occuring before

Table 2: Requirements for pipe design case study

Flowrate, Q (m^3/s)	0.5
Inner Radius, R (mm)	≥ 10, ≤ 500
Pipe Thickness, e (mm)	≥ 1, ≤ 24
Valve Closure Time, T_c (s)	≥ 0, ≤ 0.05
Peak operating pressure, P (MPa)	≤ 1
Peak axial stress, σ_x (MPa)	≤ 70 (Grade 1.4301 Steel with safety factor = 3)
Mass of pipe, M_{pipe} (kg)	≤ 3000

$t = 0.1$ s showing a design which complies with the constraint of $P_{peak} \leq 70$ MPa, however the peak pressure after 0.1 seconds gives a stress of 83 MPa. This can be explained that the design is optimized for the simulation times before 0.1 s and since the peak happens after 0.1 s, the actual peak pressure is slightly larger but given the safety factor of 3, the design is still well within safety limits.

Table 3: Parameters and performance for final design

Inner Radius, R (mm)	500
Pipe Thickness, e (mm)	1.44
Valve Closure Time, T_c (s)	0.05
Peak operating pressure, P (MPa)	0.34
Peak axial stress, σ_x (MPa)	83
Mass of pipe, M_{pipe} (kg)	724

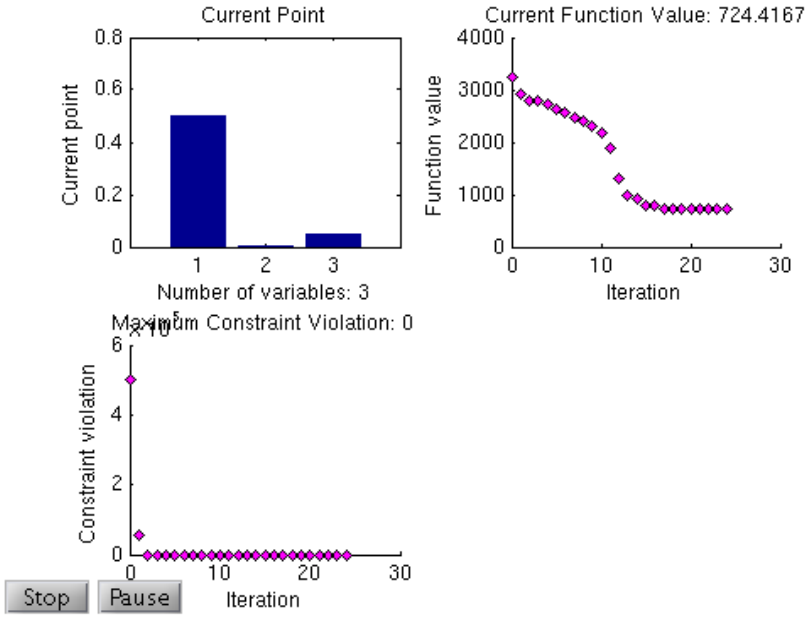

Figure 21: Optimization algorithm output plots as the optimization routine visits each potential design points (*Clockwise from top left*: Final point parameter values, Mass of different designs, Deviation from maximum constrains by the different designs)

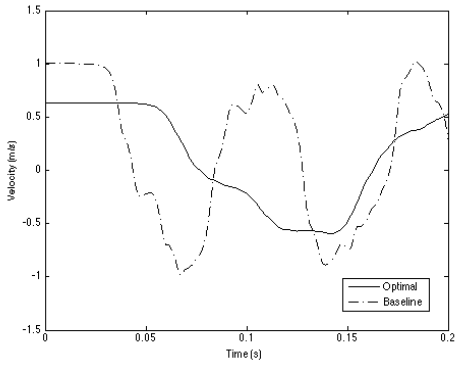

Figure 22: Internal fluid velocity at x = 11.15 m (Optimized and baseline comparison)

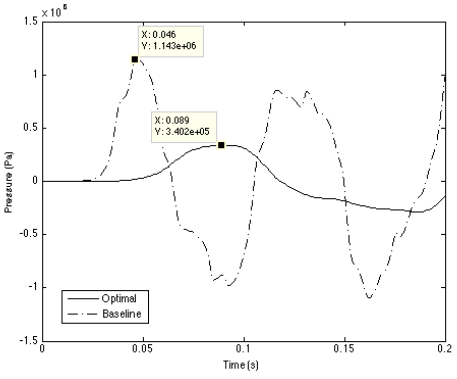

Figure 23: Fluid pressure at x = 11.15 m (Optimized and baseline comparison)

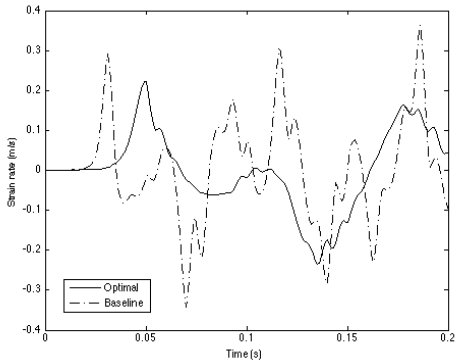

Figure 24: Pipe strain rate at x = 11.15 m (Optimized and baseline comparison)

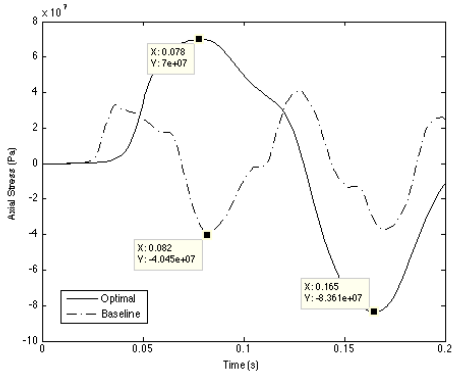

Figure 25: Pipe axial stress at x = 11.15 m (Optimized and baseline comparison)

5 Conclusion

As a summary, the exact solution for the full 1-D FSI model is presented. The new approach is shown to be slow for large simulation times but accurate due to the meshless feature. Also, the algorithm is simple to implement and highly parallelizable. The results from the Delft Hydraulics Problems show that the actual phenomenon are more realistically captured, and the peaks predicted by a standard fluid model alone is not sufficient to predict the actual phenomenon. A Fourier spectral analysis was also performed on the variables to obtain the natural frequencies of the system. However, this method might not be an ideal method for optimization studies since the long computation times to account for all the waves in the domain might prohibit the optimization of the design at longer simulation times. A better use of this method is to generate test cases and benchmark solutions for numerical methods.

Acknowledgments

The authors are grateful to Prof. Arnold Heemink for his lectures and dr. Arris Tijsseling for the project supervision, which were necessary to complete this project. The primary author would also like to thank Miss Shruti Pavagadhi for several out-of-class discussions which gave the necessary motivations and support to the primary author for the completion of this project.

References

[1] Kundu, P.K., Cohen, I.M., & Dowling, D.R. *Fluid Mechanics*, Academic Press, 5th Ed., USA, 2011.

[2] Tijsseling, A.S. *Exact solution of linear hyperbolic four-equation system in axial liquid-pipe vibration*, Journal of Fluids and Structures, No. 10, pp. 179 - 196, 2003.

[3] Skalak, R. An extension of the theory of waterhammer, Water Power, No. 7, 458-462/8,17-22, 1955.

[4] LeVeque, R.J. *Finite Volume Methods for Hyperbolic Problems*, Cambridge Texts in Applied Mathematics, Cambridge University Press, UK, 2002.

[5] Wylie, E.B. & Streeter, V.L. *Fluid Transients in Systems*, Prentice Hall, Englewood Cliffs, NJ, USA, 1993.

[6] van Rij, A.A. *Standaard afsluiterkarakteristieken (Standard valve characteristics)*, Delft Hydraulics Laboratory, Report V 195, Delft, the Netherlands, October 1970.

[7] Schedelberger, J. *Closing characteristics of spherical valves*, 3R International 14, 1975.

[8] Lavooij, C.S.W. & Tijsseling, A.S. *FLUSTRIN Phase 1 - Fluid-structure interaction in MDOF pipe systems*, Report J0252/J0284, Vol. 1: Results, May, Vol. 2: Theory, June, Delft Hydraulics, Delft, the Netherlands, 1988.

[9] Quinn, M. *Parallel Programming in C with MPI and OpenMP*, 1st Ed., McGraw-Hill Science/Engineering/Math Series, USA, 2003.

[10] *MATLAB, Optimization Toolbox, and Parallel Computing Toolbox Release 2008b*, The MathWorks, Inc., Natick, MA, USA, 2008.

[11] Intel Inc. *Intel Turbo-Boost Technology* `http://www.intel.com/technology/turboboost/index.htm`, Retrieved April 28, 2013.

A Derivation of Common Water-Hammer Fluid Equations

This section represents the views and derivation exercises solely by the primary author.

The conservation of mass, and momentum of a fluid can be described by the fully compressible Navier-Stokes equation. For this derivation, it is assumed that there exists no body forces acting on the fluid volume. The full equations are repeated here again.

$$\frac{\partial \rho}{\partial t} + \nabla \cdot (\rho \vec{V}) = 0 \tag{A.1}$$

$$\frac{\partial \rho \vec{V}}{\partial t} + \nabla \cdot \left(\rho \vec{V} \otimes \vec{V}\right) + \nabla P = \mu \nabla \cdot \left(\nabla \vec{V} + \left(\nabla \vec{V}\right)^T\right) \tag{A.2}$$

In order to determine the importance of each physical term for simplification, it is intuitive to scale and non-dimensionalize equations (A.1), and (A.2). The following are the parameters that will be used:

$$x_i^* = \frac{x_i}{L_0} \qquad \rho^* = \frac{\rho}{\rho_0} \qquad \vec{V}^* = \frac{\vec{V}}{V_0}$$

$$\nabla^* = L_0 \nabla \qquad t^* = \frac{c}{L_0} t \qquad P^* = \frac{P}{P_0}$$

where V_0 is the reference fluid speed, ρ_0 is the reference fluid density, L_0 is the reference length for the problem (in this case, it refers to the length of the pipe), and c is the speed of sound in the fluid. Since this is an acoustic wave problem, hence, in order to capture pressure waves in the fluid, the time variable is scaled with respect to the time taken for a sound wave to travel along the pipe.

Starting with equation (A.1), applying chain rule, and assuming that the fluid bulk modulus is isotropic, gives

$$\frac{\partial \rho}{\partial t} + \nabla \cdot (\rho \vec{V}) = \frac{\partial \rho}{\partial P} \frac{\partial P}{\partial t} + \rho \nabla \cdot \vec{V} + \vec{V} \cdot \left(\frac{\partial \rho}{\partial P} \mathbf{I} \nabla P\right) = 0 \tag{A.3}$$

By definition, we know that $c^{-2} = \frac{\partial \rho}{\partial P} = \frac{\rho}{K_{eff}}$, so,

$$\frac{1}{c^2}\left(\frac{\partial P}{\partial t} + \vec{V}\cdot\nabla P\right) + \rho\nabla\cdot\vec{V} = 0 \tag{A.4}$$

Apply scaling, and introduce Mach number, $M = U_0/c$, to obtain

$$\frac{P_0}{c^2}\left(\frac{\partial P^*}{\partial t^*} + M\,\vec{V}^*\cdot\nabla^* P^*\right) + \rho_0 M\,\rho^*\nabla^*\cdot\vec{V}^* = 0 \tag{A.5}$$

$$\frac{P_0}{c^2}\left(\frac{\partial P^*}{\partial t^*} + \cancel{M\,\vec{V}^*\cdot\nabla^* P^*}\right) + \rho_0 M\,\rho^*\nabla^*\cdot\vec{V}^* = 0 \tag{A.6}$$

$$\frac{P_0}{c^2}\frac{\partial P^*}{\partial t^*} + \rho_0 M\,\rho^*\nabla^*\cdot\vec{V}^* = 0 \tag{A.7}$$

The term involving the non-dimensional gradient of P drops out since the Mach number for liquid in this application is approximately 0. As an example for this project, V_0 is usually in the order of 1 m/s, and the speed of sound in water is approximately of the order of 1000 m/s. Hence the Mach number is only of the order 10^{-3}. But the time derivative term cannot be ignored since the reference pressure, P_0 is usually in the order of 10^5.

Doing the same for the momentum equation gives,

$$\frac{\partial \rho^*\vec{V}^*}{\partial t^*} + \frac{V_0}{c}\nabla^*\cdot\left(\rho^*\vec{V}^*\otimes\vec{V}^*\right) + \frac{P_0}{V_0\rho_0 c}\nabla^* P^* = \frac{\mu}{L_0\rho_0 c}\nabla^*\cdot\left(\nabla^*\vec{V}^* + \left(\nabla^*\vec{V}^*\right)^T\right) \tag{A.8}$$

$$\frac{\partial \rho^*\vec{V}^*}{\partial t^*} + \cancel{M\nabla^*\cdot\left(\rho^*\vec{V}^*\otimes\vec{V}^*\right)} + \frac{P_0}{V_0\rho_0 c}\nabla^* P^* = \cancel{\frac{1}{Re_c}\nabla^*\cdot\left(\nabla^*\vec{V}^* + \left(\nabla^*\vec{V}^*\right)^T\right)} \tag{A.9}$$

$$\frac{\partial \rho^*\vec{V}^*}{\partial t^*} + \frac{P_0}{V_0\rho_0 c}\nabla^* P^* = 0 \tag{A.10}$$

$$\vec{V}^*\frac{\partial \rho^*}{\partial P^*}\frac{\partial P^*}{\partial t^*} + \rho^*\frac{\partial \vec{V}^*}{\partial t^*} + \frac{P_0}{V_0\rho_0 c}\nabla^* P^* = 0 \tag{A.11}$$

$$\cancel{\frac{1}{c^2}\vec{V}^*\frac{\partial P^*}{\partial t^*}} + \rho^*\frac{\partial \vec{V}^*}{\partial t^*} + \frac{P_0}{V_0\rho_0 c}\nabla^* P^* = 0 \tag{A.12}$$

$$\rho^*\frac{\partial \vec{V}^*}{\partial t^*} + \frac{P_0}{V_0\rho_0 c}\nabla^* P^* = 0 \tag{A.13}$$

The non-dimensional form of the water hammer equations are thus given by

$$\frac{P_0}{c^2}\frac{\partial P^*}{\partial t^*} + \rho_0 M\, \rho^* \nabla^* \cdot \vec{V}^* = 0 \tag{A.14}$$

$$\rho^* \frac{\partial \vec{V}^*}{\partial t^*} + \frac{P_0}{V_0 \rho_0 c}\nabla^* P^* = 0 \tag{A.15}$$

Converting the equations back to the dimensionalized form, gives the frequently used water hammer equations [Equations (A.16) & (A.17)].

$$\frac{1}{K_{eff}}\frac{\partial P}{\partial t} + \nabla \cdot \vec{V} = 0 \tag{A.16}$$

$$\frac{\partial \vec{V}}{\partial t} + \frac{1}{\rho}\nabla P = 0 \tag{A.17}$$

The whole derivation exercise seeks to explicitly show as well as to refute arguments from the project presentation by a stubborn guest, from conservation laws, the physics and assumptions involved to obtain the water hammer equations. This is especially important since even an expert in water applications can get the physics wrong by first assuming that a liquid is fully incompressible. By making such ignorant assumptions, then, the pressure waves cannot be captured by the model. It is clearly shown in this exercise that the fluid is only slightly compressible but not totally incompressible.